

# Preclinical activity of fluvastatin-loaded self-nanoemulsifying delivery system against breast cancer models: Emphasis on apoptosis

Hanan Elimam<sup>1,2</sup>  | Jihan Hussein<sup>3</sup> | Yasmin Abdel-Latif<sup>3,4</sup> | Amal Kamal Abdel-Aziz<sup>5</sup> | Khalid M. El-Say<sup>6</sup> 

<sup>1</sup>Department of Biochemistry, Faculty of Pharmacy, University of Sadat City, Sadat City, Egypt

<sup>2</sup>Department of Biochemistry, Faculty of Pharmacy, Sinai University, Kantara, Egypt

<sup>3</sup>Department of Medical Biochemistry, National Research Centre, Giza, Egypt

<sup>4</sup>Faculty of Biotechnology, October University for Modern Sciences and Arts (MSA), 6th of October, Giza, Egypt

<sup>5</sup>Department of Pharmacology and Toxicology, Faculty of Pharmacy, Ain Shams University, Cairo, Egypt

<sup>6</sup>Department of Pharmaceutics, Faculty of Pharmacy, King Abdulaziz University, Jeddah, Saudi Arabia

## Correspondence

Hanan Elimam, Department of Biochemistry, Faculty of Pharmacy, University of Sadat City, Sadat City 32958, Egypt.

Email: [Hanan.Elimam@fop.usc.edu.eg](mailto:Hanan.Elimam@fop.usc.edu.eg)

## Abstract

Statins trigger apoptotic cell death in some types of growing tumor cells in a cholesterol-lowering-independent manner. Self-nanoemulsifying delivery systems (SNEDs) are potentially effective for the suppression of breast cancer development. This study aims to investigate the potential anticancer activity of fluvastatin (FLV)-SNEDs in breast cancer while comparing it with FLV in vitro as well as in vivo exploiting/using MDA-MB-231 and Ehrlich ascites carcinoma (EAC)-bearing mice, respectively. Biochemical analysis of liver and kidney functions, oxidative stress markers, and histopathological examinations of such tumor tissues were performed showing the potentiality of SNEDs as a nanocarrier for antitumor agents. FLV-SNEDs demonstrated more potent anticancer activity compared to FLV on MDA-MB-231 and hepatocellular carcinoma (HepG2) cells. In vivo experiments on the EAC-bearing mice model indicated that FLV and—to a greater extent—FLV-SNEDs ameliorated EAC-induced hepatotoxicity and nephrotoxicity. FLV or FLV-SNEDs evidently reduced the percent of Ki-67 +ve EAC cells by 57.5% and 86.5% in comparison to the vehicle-treated EAC group. In addition, FLV or FLV-SNEDs decreased Bcl-2 levels in serum and liver specimens. In contrast, FLV or FLV-SNEDs significantly activated the executioner caspase-3. Simultaneously, both FLV and FLV-SNEDs stimulated p53 signaling and modulated Bcl-2 protein levels in treated cells. Collectively, these results support the contribution of apoptotic cell death in mediating the anticancer activities of FLV and FLV-SNEDs against murine EAC model in vivo. This study provides new understandings of how FLV and FLV-SNEDs regulate EAC cell viability via upregulation of p53 signaling, and through modulation of cleaved caspase-3 as well as antiapoptotic Bcl-2 marker.

**Abbreviations:** Bcl-2, B-cell lymphoma 2; BUN, Blood urea nitrogen; EAC, Ehrlich ascites carcinoma; FLV, fluvastatin; HepG2, hepatocellular carcinoma; HMG-CoA, 3-hydroxy-3-methyl-glutaryl coenzyme A; MAPK, mitogen-activated protein kinase; MDA-MB-231, human breast adenocarcinoma cells; NE, nanoemulsion; PI, propidium iodide; SNED, self-nanoemulsifying delivery system; TEM, transmission electron microscopy; TNBC, triple negative breast cancer.

**KEYWORDS**

apoptosis, fluvastatin, p53, self-nanoemulsifying delivery system, triple-negative breast cancer

## 1 | INTRODUCTION

Cancer is the second leading cause of death in humans worldwide. Despite the fact that an enormous effort and success was made in the “war on cancer,” many important details needed to be improved. Cancer is defined as a collection of abnormal cells that grow at a random and rapid rate due to disruption of normal cell division or apoptosis.<sup>1</sup> Mitogen-activated protein kinase (MAPK) signaling, autophagosome formation, and apoptotic signaling are recognized cellular signals that control cell division, differentiation, and cell death. In many types of cancer, ascites is a prognostic indicator of the advanced stage.

Experimental malignancies are of considerable interest for the reasons of modeling. Ehrlich ascites carcinoma (EAC) is one of the well-known models for carcinoma. It appeared for the first time, in a female mouse, as a spontaneous breast cancer.<sup>2</sup> EAC is described as hyperdiploid undifferentiated carcinoma which has a potential transplanted ability. It has a small life span, proliferates quickly, but no regression. Furthermore, EAC does not contain a tumor-specific transplantation antigen.<sup>3</sup>

Statins are a medication class that is clinically used to treat hypercholesterolemia. It decreases the blood level of cholesterol by inhibiting 3-hydroxy-3-methyl-glutaryl-coenzyme A (HMG-CoA) reductase, which is the rate-determining enzyme in the pathway of mevalonate synthesis. Dolichol, ubiquinone, geranylgeranyl pyrophosphate, and cholesterol are all end products of this pathway. Therefore, HMG-CoA reductase plays a role in a variety of cellular functions, including cell differentiation and proliferation.<sup>4–6</sup> Cholesterol is less in many cancer cell lines compared to normal cells, which could be owing to excessive utilization of cholesterol by cancer cells. The role of statins in cancer prevention or therapy has caused controversy during the last decade, but preclinical and clinical data obtained in the last decade support the use of statins in the prevention of breast cancer.<sup>7</sup> Targeting cancer cells with non-toxic therapeutic agents, which differ in the mechanisms of action, enhance the treatment efficacy. Repurposing of existing statin drugs as anticancer agents is owing to their pleiotropic effect on a variety of cells and tissues.<sup>8</sup> The mechanism through which statins may exert their anticancer effects has been studied using many breast cancer cell lines. Statins stimulate apoptosis and inhibit

tumor cell proliferation and invasion.<sup>9,10</sup> This anticancer effect could be owing to their lipid-lowering function; however, the full molecular interaction is still unknown. Several studies have investigated the implication of autophagy in carcinogenesis and progression is complicated, because inducing autophagy could either speed up or slow down the tumor progression. Only a few in vitro studies have shown that inhibiting autophagy can increase statin-induced apoptosis or cytotoxicity in various cancer cell lines.<sup>11–13</sup>

Fluvastatin (FLV), one of the HMG-CoA reductase inhibitors, demonstrates both in vitro and in vivo antitumor effects in a variety of human cancers including those of the breast,<sup>14,15</sup> lung<sup>16</sup> and colorectal cancer,<sup>17</sup> which have been related to cell cycle arrest, thereby prevention of cell proliferation and induction of apoptotic and necrotic cell death. Recently, a nanoparticle-based method has been used to develop FLV in a nanostructured system (self-nanoemulsifying delivery system; SNED) to improve the solubility and bioavailability of FLV.<sup>14</sup> The nanoparticle strategies may also be useful to protect the drug from degradation, extend its biological half-lives, manage drug release, and maximize drug efficacy. The cellular response of SNEDs-delivered FLV was examined previously in an in vitro study using a human colorectal cancer cell line (HCT116). Loading FLV into SNEDs enhanced its cellular uptake and therefore increased its cytotoxicity to colorectal carcinoma.<sup>18</sup>

The present research aimed at investigating the potential anticancer activity of FLV-SNEDs in breast cancer while comparing it with FLV in vitro as well as in vivo exploiting/using MDA-MB-231 and EAC, respectively. Also, this study aimed to explore their molecular mechanisms underlying their anticancer activities against different subtypes of cancer in vitro and in vivo EAC-bearing mouse model with an emphasis on the molecular mechanisms involving apoptosis of tumor cells.

## 2 | MATERIALS AND METHODS

### 2.1 | Materials

Fluvastatin sodium was donated as a gift from SPIMACO. Sulphorhodamine (SRB), Polyoxyethylene (20)

sorbitan monooleate (Tween 80), and polyethylene glycol 200 (PEG 200) were purchased from Sigma-Aldrich. EAC cell line was purchased from National Cancer Institute. Tissue culture media was from Invitrogen-Life Technologies. Electrophoresis reagents were from Bio-Rad Laboratories. Rabbit antibodies to cleaved-caspase-3 (Asp175; 5A1E; #9664) and Bcl-2 (#3498) were purchased from Cell Signaling Technology; rabbit anti-Ki-67 monoclonal antibody (ab16667, Abcam); rabbit anti-AKT (sc-8312, Santa Cruz Biotechnology); rabbit anti-pAKT (Ser 473; sc-33437, Santa Cruz Biotechnology); rabbit anti-actin (A2066) were from MilliporeSigma.

## 2.2 | Preparation of FLV-SNEDs

FLV-SNEDs were prepared and evaluated as reported previously in our article.<sup>14</sup> Briefly, 1 g of the SNEDs was prepared by vortexing a mixture of three components (Olive oil, Tween 80, and PEG 200) with 50 mg of FLV for 1 min till complete solubilization in the SNEDs.

## 2.3 | Evaluation of FLV-SNEDs

### 2.3.1 | Thermodynamic stability and self-emulsification ability

The thermodynamic stability was assessed by subjecting the prepared FLV-SNEDs to different tests like three cycles between heating at 45°C and cooling at 25°C, centrifugation at 500 rpm for 30 min, and three cycles of freeze and thaw (between -25 and 25°C) as the adopted procedure.<sup>19</sup> Then, the SNEDs were visually inspected for any drug precipitation, phase separation, and coalescence. The formulation that withstands the previous stress tests was further subjected to self-emulsification tests to investigate its stability upon dilution with different diluents such as water, 0.1 N HCl (pH 1.2), and phosphate buffer (pH 6.8) to mimic stomach and intestinal conditions, respectively.<sup>20</sup> To perform self-emulsification efficiency tests on FLV-SNEDs, 1 ml was sufficiently diluted (1:500) with each diluent. The potential of self-emulsification was measured using A-E grading systems reported in the literature.<sup>21,22</sup>

### 2.3.2 | Physicochemical characterization

FLV-SNEDs dispersion in 20 ml water was examined for droplet size distribution, polydispersity index (PDI), zeta potential (ZP) using a Malvern Zetasizer Nano ZSP, Malvern, Panalytical Ltd at 22°C. Light microscopy

(LeicaDM300, optical microscope), and transmission electron microscopy (TEM; 100CX; JEOL) were also used to explore the morphological features of FLV-SNEDs.<sup>14,18</sup>

## 2.4 | In vitro experiments on cancer cell lines

### 2.4.1 | Human cancer cell lines and cell culture

Human triple-negative breast adenocarcinoma (MDA-MB-231) and hepatocellular carcinoma (HepG2) cells were provided by American Type Culture Collection (ATCC) and were grown as monolayer cultures in Dulbecco's modified Eagle's medium (DMEM) supplemented with 2 mM L-glutamine, 10% fetal bovine serum, and 1% penicillin-streptomycin. After trypsinization (0.5% trypsin/2.6 mM EDTA), cells were subcultured to preconfluency in a humidified tissue culture incubator at 37°C with 5% CO<sub>2</sub>.

### 2.4.2 | Sulphorhodamine B cytotoxicity assay

As previously described, cell proliferation was assessed using the sulphorhodamine B (SRB) cytotoxicity assay.<sup>23,24</sup> Cells were plated into 96-well plates. After 24 h, one set of the plates of each cell line was fixed with trichloroacetic acid to reflect the basal cell population for each cell line at the time of drug treatment (i.e., at time zero ( $T_z$ )). In another set of plates, cells were treated with varying concentrations of FLV or FLV-SNEDs for 24 h. Cells were then fixed with ice-cold 50% trichloroacetic acid for 1 h at 4°C and stained with 50  $\mu$ l 0.4% SRB for 30 min at room temperature. SRB was dissolved in 10 mM Tris buffer. GloMax<sup>®</sup> multimicroplate reader was used to measure the optical density (O.D.) at 560 nm. The survival fraction was estimated as follows: O.D. (drug-treated cells)/O.D. (untreated cells). Percentage growth inhibition (% GI) was calculated as follows:  $[(T_i - T_z)/(C - T_z)] \times 100$  for concentrations where  $T_i \geq T_z$  and  $[(T_i - T_z)/T_z] \times 100$  for concentrations where  $T_i < T_z$  ( $C$  and  $T_z$  correspond to the absorbance of vehicle and drug-treated cells following the indicated time of treatment, respectively).

### 2.4.3 | Quantification of cell death

Twenty-four hours following their treatment, MDA-MB-231 cells were collected by trypsinization, washed with phosphate-buffered saline (PBS; pH 7.2), and then

stained with propidium iodide (10 mg/ml). Cell fluorescence was quantified with a flow cytometer (FACSCalibur; Becton Dickinson) and analyzed with FlowJo software as previously described.<sup>25</sup>

## 2.5 | In vivo experiments on mice

### 2.5.1 | Animals

Five-week-old female Swiss albino mice (20–25 g) were obtained from an animal house of the National Cancer Research Institute. They were kept in stainless steel cages at a temperature of 25°C and 55% humidity. Mice were maintained in-house with 12 h on-off light cycles day length with standard laboratory diet and water ad libitum at the animal house of the National Research Centre. All methods were performed in accordance with the relevant guidelines of the ethical care, the experimental design and treatment of the animals followed the regulations of the National Research Centre's ethical committee in Dokki, Cairo, Egypt.

### 2.5.2 | Experimental study design

Forty healthy Swiss albino mice were randomly divided into four groups (10 mice each): Group I (control) which were healthy mice treated daily with normal saline, Group II (EAC model) mice were injected with EAC cells intraperitoneally for induction of ascites tumor, Group III (FLV) which were EAC mice treated daily with 20 mg/kg of FLV, 1 day after tumor inoculation, and Group IV (FLV-SNEDs) which were EAC mice treated daily with 20 mg/kg of FLV-SNEDs, 1 day after tumor inoculation. This dose of FLV was chosen based on previous preclinical studies and was expected to be within therapeutic activity of FLV. All groups were treated for 2 weeks (Figure 3A).<sup>16,26</sup>

### 2.5.3 | In vivo EAC-bearing model

To induce EAC in mice for the experimental study, briefly and as previously reported, EAC cells were implanted into mice through intraperitoneal injection of ( $2.5 \times 10^6$  of EAC/mouse); tumor appeared 5–7 days following EAC cell inoculation.<sup>3</sup>

### 2.5.4 | Blood and tissue sampling

At the end of the experiment, animals were kept fasting for 12 h, blood was taken from the retro-orbital venous

plexus of the eye while the animals were under light anesthesia. Blood is allowed to coagulate at 37°C, centrifuged at 4000 rpm for 15 min in a cooling centrifuge. Serum was isolated and separated into aliquots then kept at –20°C for biochemical examination.<sup>27</sup> Mice were killed by decapitation, the liver was promptly removed from each mouse then perfused with ice-cold PBS (pH 7.4) to remove blood. Each liver was isolated, the left lobe was used for pathological examination and the other lobe was cut into small pieces, only 0.5 g of them was homogenized in 2 ml PBS (pH 7.4), centrifuged at 4000 rpm for 15 min at 4°C and the supernatant was collected for the assessment of biochemical parameters.<sup>3</sup> The remaining pieces of the second lobe were used for western immunoblotting analysis.

## 2.6 | Histopathology

The left lobe of mouse liver tissues was collected, fixed in 10% saline formalin then dehydrated with ethanol. The fixed liver specimens were embedded in paraffin. Sections (5- $\mu$ m thick) were stained with hematoxylin-eosin and observed by light microscopy.<sup>28</sup>

## 2.7 | Immunohistochemistry

Automated immunohistochemistry (IHC) was performed using Ventana Discovery Ultra instrument (Roche) at the Histopathology Platform, Research Institute of the McGill University Health Centre. A standard protocol and specific antibodies against Ki-67 and cleaved caspase-3 were used. Briefly, formalin-fixed, paraffin-embedded liver tissue sections (4  $\mu$ m) were used for the immunohistochemical analyses. They were deparaffinized, rehydrated, and blocked with inhibitor CM for endogenous peroxidase activity. The standard antigen retrieval method is performed using heat-induced epitope retrieval in Tris-EDTA buffer (pH 7.8) at 95°C for 44 min. The sections were then incubated at 37°C for 24 min with corresponding primary antibodies as follows, rabbit anti-Ki-67 monoclonal antibody and anti-cleaved caspase-3. After washing, slides were incubated with the secondary antibodies (anti-Rabbit HRP, 20 min). The Discovery ChromoMap DAB Kit (Cat #760-159, Roche) was used to detect positive signals. DAB kit for Ki-67 (purple) and cleaved caspase-3 (brown) chromogens were applied for 8 min at room temperature to detect the signal.<sup>29</sup>

After IHC staining, the slides were washed, and sections were counterstained with hematoxylin and bluing reagent for 4 min each. Stained slides were

washed, dehydrated, and mounted in a mounting media. Finally, slides were digitally scanned, and photographs of stained sections were captured by ImageScope software (Leica) with a 20× objective.<sup>30</sup> The results are expressed as the percentage of positively stained cells in 10–12 randomly selected microscopic fields.<sup>31</sup>

## 2.8 | Biochemical analysis

Aspartate aminotransferase (AST) and Alanine aminotransferase (ALT) were determined following the method described by Reitman and Frankel by using a commercial kit purchased from BioMed Diagnostics.<sup>32,33</sup> The level of blood urea was measured colorimetrically as reported previously<sup>34</sup> and serum creatinine was measured by the kinetic method described in Laesn.<sup>35</sup> Liver homogenates were used for estimation of the levels of malondialdehyde (MDA) by Ohkawa et al. protocol<sup>36</sup> and nitric oxide (NO) according to the method of Moshage et al.<sup>37</sup> The activity of catalase (CAT) was determined using the procedures described by Johansson et al.<sup>38</sup>

## 2.9 | Enzyme-linked immunosorbent assay

Plasma B-cell lymphoma 2 (Bcl-2) serum level was assayed by enzyme-linked immunosorbent assay technique using Bcl-2 assay kit purchased from R&D Systems GmbH. The assay was conducted in accordance with the instructions provided with Bcl-2 assay kit.

## 2.10 | Total RNA isolation and cDNA synthesis

Total RNA was isolated from tissues of treated groups using TriZol (Invitrogen) and chloroform procedures. Samples were adjusted to final concentrations of 100 ng/ml after dissolving RNA in RNase-free water. 10 µl from each sample of purified RNA was used to make cDNA using a cDNA synthesis kit (QIAGEN). Total RNA was incubated with reverse transcriptase and oligo-(dT) primers at 45°C for 1 h, followed by a 5-min incubation at 95°C, according to the manufacturer's instructions. cDNA was kept at -20°C until analysis.<sup>39</sup>

## 2.11 | Quantitative real-time PCR assay

Quantitative real-time PCR was used to estimate the expression levels of Bcl-2 (B-cell lymphoma 2) gene in

isolated cells from liver tissues. cDNA was employed as a template for PCR amplification with DNA polymerase and specific primers for Bcl-2. Quanti-Tect SYBR Green PCR Kit (QIAGEN) was used to determine the relative gene expression of Bcl-2. Oligonucleotides specific for Bcl-2 gene were designed with Primer Express software (version 2.0), F: 5'-CGGGAGAACAGGGTATGA-3' and R: 5'-CAGGCTGGAAGGAGAAGAT-3'. The previous gene was normalized on the expression values of β-actin gene (β-actin-F: 5'-CCCCATCGAGCACGGTAT TG-3', β-actin-R: 5'-ATGGCGGGGGTGTGAAGGTC-3'). The real-time PCR reaction was carried out in an Applied Bio-system instrument, at a 50°C for 2 min and 95°C for 10 min followed by 40 cycles of 95°C for 30 s, annealing at 60°C for 30 s, and extension at 72°C for 30 s. The threshold cycle (C<sub>T</sub>) values were analyzed using SDS 2.2.<sup>40</sup>

## 2.12 | Western immunoblotting

Isolated liver tissues or harvested cells were lysed in ice-cold lysis buffer comprising 1% Triton X-100, 10 mM Tris, pH 7.4, 1 mM EGTA, 125 mM NaCl, 2 mM Na<sub>3</sub>VO<sub>4</sub>, 25 mM NaF, and 10 mM sodium pyrophosphate, supplemented with a mixture of protease inhibitor. Protein concentrations were determined using Bradford assays after centrifugation of the lysates at 13 000 rpm for 10 min. Lysate proteins were dissolved in Laemmli buffer and separated by SDS-PAGE. Proteins were transferred to polyvinylidene difluoride membranes by electrophoresis. Membranes were blocked at 22°C for 1 h with 5% bovine serum albumin (BSA) in 1× Tris-buffered saline with 0.1% Tween 20. Membranes were incubated overnight with primary antibodies in 5% BSA, followed by 1-h incubation at 22°C with goat anti-rabbit IgG horseradish peroxidase-conjugated secondary antibody. Membranes were developed with ECL.<sup>39,41</sup> ImageJ software was used to perform quantitative densitometry of protein bands (National Institutes of Health).<sup>42</sup>

## 2.13 | Statistical analysis

Results were measured in triplicates taking the error bars into account. One-way ANOVA was used to analyze the current data (mean ± SE). Where significant differences were found, individual comparisons were made between groups using Tukey's method (post hoc analysis). Two-way ANOVA followed by Bonferonni post hoc test was used to analyze the results of some

experiments (GraphPad Prism, version 8.4.2). Statistical significance was defined as a probability value of  $<0.05$ .

### 3 | RESULTS

#### 3.1 | Evaluation of the FLV-SNEDs

The prepared FLV-SNEDs displayed thermodynamic stability at different stress conditions like heating and cooling cycles, centrifugation, and freeze and thaw cycles. Also, it was found that FLV-SNEDs passed the self-emulsification test with grade A upon dilution with three different diluents which indicated the self-emulsification within 1 min and produced clear/translucent nanoemulsion. FLV-SNEDs droplet size showed a unimodal distribution with a PDI value of 0.29 and an average size of  $162.3 \pm 57$  nm (Figure 1A). This nanosize represents the key element that affects *in vivo* absorption across membranes, and uptake into biological systems. Also, the zeta potential was  $-27.1$  mV, which indicates the physicochemical stability of the formulation (Figure 1B). Moreover, optical and TEM images (Figure 1C,D) showed almost spherical particle morphology in the aqueous medium, indicating that FLV-SNEDs

form homogeneous nanoscale structures and confirm the uniformity of size.

#### 3.2 | FLV and FLV-SNEDs impede the viability of triple-negative breast cancer and hepatocellular carcinoma cells *in vitro*

We have previously demonstrated that a novel nanosized FLV formula (FLV-SNEDs) exhibited potent anticancer activity against MCF-7 breast cancer cell line which expresses estrogen (ER), progesterone (PR), and glucocorticoid receptors.<sup>14</sup> In this study, we sought to assess the potential anticancer activity of FLV-SNEDs against other aggressive subtypes of cancer with limited treatment options as triple-negative breast cancer (TNBC). To this end, we investigated the cytotoxic activity of FLV and FLV-SNEDs on MDA-MB-231, a highly aggressive, invasive, and poorly differentiated TNBC cell line which does not express estrogen receptor (ER), progesterone receptor (PR), and human epidermal growth factor receptor 2 (HER2/Neu) amplification. We initially tested the effect of varying concentrations of FLV and FLV-SNEDs on the survival and proliferation of MDA-MB-231 cells using Sulphorhodamine B (SRB) assay.<sup>43</sup> SRB assay

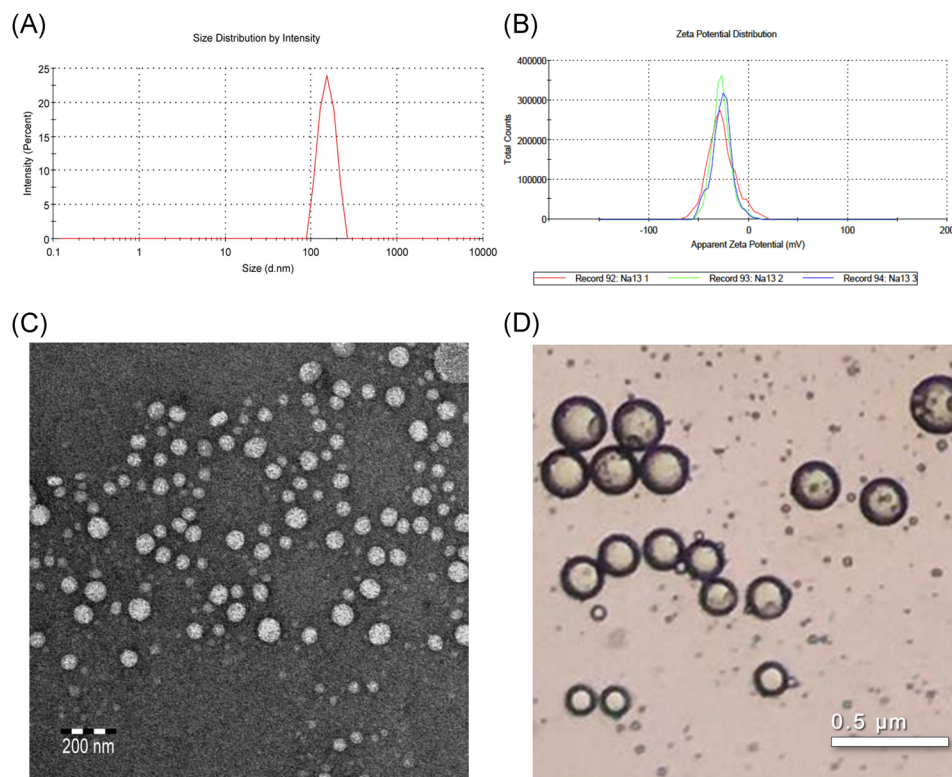


**FIGURE 1** Characterization of FLV-SNEDs. Particle size (A), zeta potential (B) distribution were measured by particle size analyzer and photomicrographs of the FLV-SNEDs were acquired by TEM (C), and optical microscope images at 400× magnification power (D). FLV, fluvastatin; SNED, self-nanoemulsifying delivery system; TEM, transmission electron microscopy

is a high-throughput assay adopted by the National Cancer Institute in the NCI-60 screening. SRB assay is based on the colorimetric evaluation of the SRB dye bound to basic amino acids of cellular proteins and thereby provides an estimate of total protein mass, and cell number. Indeed, FLV-SNEDs significantly reduced the survival and proliferative potential of MDA-MB-231 cells in a concentration-dependent pattern as compared to vehicle and FLV-treated cells (Figure 2A,B). We next questioned whether cancer cells belonging to types other than breast cancer are more responsive to FLV-SNEDs compared to FLV. Consistently, FLV-SNEDs demonstrated more potent anticancer activity compared to FLV on hepatocellular carcinoma (HepG2) cells (Figure 2C,D). Altogether, these findings emphasize the anticancer activity of FLV-SNEDs on diverse types of cancer *in vitro*.

Apoptotic and necrotic cell death have been reported as key effectors mediating the anticancer activity of diverse therapies including drug-loaded SNEDs.<sup>14</sup> To explore the potential involvement of apoptosis and necrosis in FLV and FLV-SNED-induced cytotoxicity, we exploited propidium Iodide (PI), a fluorescent cell impermeable nuclear dye which is excluded by viable and early apoptotic cells. However, it penetrates the cell membrane of necrotic or late apoptotic cells.<sup>44,45</sup> Interestingly, FLV-SNEDs significantly increased the percent of apoptotic and necrotic of MDA-MB-231 cells as compared to FLV and vehicle-treated cells (Figure 2E). p53 is a tumor suppressor protein, which can trigger apoptotic cell death in response to various chemotherapeutic agents and radiotherapy.<sup>46</sup> Immunoblot analysis revealed that FLV-SNEDs significantly increased p53 levels as compared to vehicle and FLV-treated MDA-MB-231 cells (Figure 2F,G). Altogether, these findings indicate that this late-apoptotic event in FLV-SNEDs-treated MDA-MB-231 cells might be mediated by the p53-dependent pathway.

### 3.3 | FLV and FLV-SNEDs evidently impair the growth of murine mammary adenocarcinoma model *in vivo*

In light of the present *in vitro* data, we sought to further validate the antitumor activities of FLV and FLV-SNEDs in EAC, a murine mammary adenocarcinoma model *in vivo*. Following their intraperitoneal transplantation with EAC, mice were randomly assigned into three different treatment cohorts: vehicle, FLV, and FLV-SNEDs (Figure 3A). A fourth cohort included the control mice which were not transplanted by EAC. The anticancer efficacies of FLV and FLV-SNEDs in treating

EAC-transplanted mice were assessed by monitoring the body weight and volume of ascitic fluid (Figure 3B,C). Fifteen days postinoculation of EAC, the body weight and volume of the ascitic fluid of vehicle-treated transplanted mice significantly were increased by 25% and 400%, respectively, as compared to control (non-EAC transplanted) mice (Figure 3B,C). In contrast, FLV and—to a greater extent—FLV-SNEDs significantly attenuated EAC-associated increment in the body weight and ascitic fluid volume of treated mice to a level corresponding to that of control mice (Figure 3B,C).

### 3.4 | FLV and FLV-SNEDs counteract EAC-induced hepatotoxicity and nephrotoxicity

Ehrlich ascites carcinoma (EAC) is a spontaneous mammary adenocarcinoma model which metastasizes to distinct organs including the liver.<sup>47</sup> Hence, we first questioned the impact of the metastasizing EAC cells on the histoarchitecture and function of normal hepatocytes. Second, we explored whether FLV and FLV-SNEDs could reverse/abrogate the impact of EAC on the characteristic cord-like arrangement of the hepatocytes. To this end, we initially performed a histopathological examination of liver specimens of different cohorts (Figure 3D). In line with a previously published study,<sup>46</sup> histopathological examination revealed that control (non-EAC transplanted) mice have normal liver cords and liver sinusoids. However, vehicle-treated EAC-transplanted mice showed cohesive groups of malignant epithelial cells with malignant features (nuclear hyperchromatism and pleomorphism), and sinusoidal congestion as shown in Figure 3D. Liver sections of FLV- or FLV-SNEDs-treated EAC-transplanted groups appeared to be normal without any tumor cell infiltration. Treatment of EAC-transplanted mice with FLV improved the liver histopathological feature and showed high-grade dysplastic changes. Cells were with hyperchromatic nuclei and prominent nucleoli. FLV-SNEDs-treated EAC-transplanted mice showed complete recovery of the affected liver with mild large cell atypia and normal sinusoids (Figure 3D).

Moreover, the liver function was evaluated by assessing serum ALT and AST levels which are broadly used as biomarkers of hepatocellular injury. As outlined in Table 1, hepatotoxicity was evident in vehicle-treated EAC-transplanted mice as indicated by the elevated levels of serum ALT and AST levels (by  $\approx 70\%$  and  $50\%$ , respectively, as compared to normal control (non-EAC transplanted) mice). FLV and FLV-SNEDs significantly reduced serum AST levels as compared to vehicle-treated

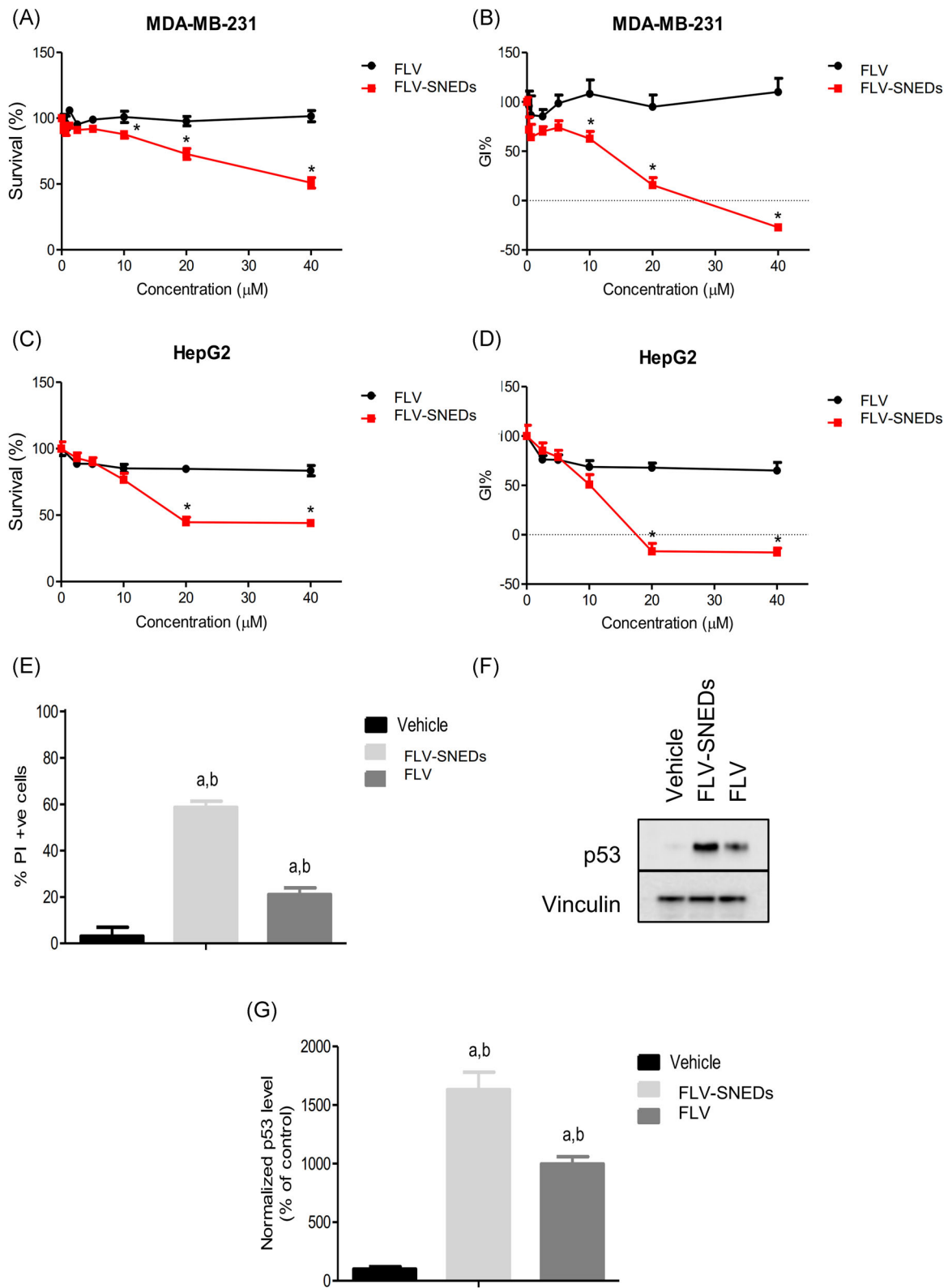


FIGURE 2 (See caption on next page)



EAC transplanted mice (Table 1). Notably, while FLV and FLV-SNEDs attenuated EAC-induced increment in serum ALT levels, FLV-SNEDs counteracted EAC-associated elevation in serum ALT levels restoring their levels to that of normal (non-EAC transplanted) cohort (Table 1). The kidneys are also among the organs to which EAC metastasizes.<sup>47</sup> Indeed, the levels of blood urea nitrogen (BUN) and serum creatinine were dramatically increased in the vehicle-treated EAC transplanted mice by approximately 137% and 70%, respectively, as compared to the control cohort (Table 2). Consistently, FLV and FLV-SNEDs significantly attenuated EAC-induced increment in serum creatinine levels by almost 30% and 50%, respectively, when compared to the vehicle-treated EAC group. It is worth mentioning that while FLV and FLV-SNEDs significantly counteracted EAC-associated increase in BUN levels, FLV-SNEDs treatment effectively restored the normal physiological levels of BUN (Table 2). Collectively, these findings indicate that the anticancer activity of FLV and—to a greater extent—FLV-SNEDs ameliorate EAC-induced hepatotoxicity and nephrotoxicity.

### 3.5 | FLV and FLV-SNEDs guard against EAC-induced perturbation of hepatic antioxidant defense mechanisms

The growing and metastasizing EAC cells have been reported to generate massive amounts of free radicals which are thought to contribute to EAC-induced hepatotoxicity. Free radicals trigger lipid peroxidation and malondialdehyde (MDA) is one of the final products of polyunsaturated fatty acids peroxidation. Consistently, EAC significantly increased the MDA levels by approximately 191% in liver tissues as compared to the control (non-EAC transplanted) group (Table 3). FLV and FLV-SNEDs significantly reduced EAC-associated elevation in MDA levels by  $\approx$ 41% and 44%, respectively. Notably, treatment of EAC-transplanted mice with FLV-SNEDs

effectively negated EAC-induced lipid peroxidation as evidenced by restoring the physiological levels of MDA.

Excessive production of nitric oxide (NO) has been reported to exacerbate oxidative stress through the formation of reactive nitrogen species (RNS) which in turn induce cellular injury via distinct mechanisms such as peroxidation of membrane lipids, proteins, and DNA. In accordance with increased lipid peroxidation, NO levels were significantly increased by approximately 170% in the liver homogenates of vehicle-treated EAC transplanted cohort (Table 3). FLV and FLV-SNEDs drastically reduced NO levels in the liver homogenate by 22% and 38%, respectively, as compared to vehicle-treated EAC transplanted mice (Table 3).

Catalase (CAT) is one of the fundamental antioxidant enzymes which catalyzes the conversion of hydrogen peroxide ( $H_2O_2$ ) into water and molecular oxygen. Hence, CAT guards the cells against the cytotoxic damage induced by free radicals. In line with the inhibitory effect of NO on CAT,<sup>48</sup> EAC reduced CAT activity in liver homogenates by approximately 65% as compared to the control (non-EAC transplanted) cohort (Table 3). Treatment with FLV or FLV-SNEDs counteracted EAC-mediated inactivation of CAT as evidenced by its increased activity by  $\approx$ 44% and 147%, respectively, as compared to vehicle-treated EAC-transplanted cohort (Table 3). Altogether, our results emphasize the pro-oxidant hepatotoxic effects of EAC which is effectively attenuated by the administration of FLV or FLV-SNEDs.

### 3.6 | FLV and FLV-SNEDs trigger apoptotic cell death of EAC in vivo

Evaluation of breast cancer proliferation presents one of the crucial prognostic factors. Ki-67 is a nuclear protein that is present during all phases of the cell cycle except for quiescent G<sub>0</sub>, and hence it reflects the proportion of

**FIGURE 2** The effects of FLV and FLV-SNEDs on the survival and proliferation of human triple-negative breast cancer (MDA-MB-231) and hepatocellular carcinoma (HepG2) cells. (A, B) Percent of survival (A) and growth inhibition (B) of MDA-MB-231 cells treated with the indicated concentrations of FLV and FLV-SNEDs for 24 h and assessed using Sulphorhodamine B (SRB) cytotoxicity assay. (C, D) Percent of survival (C) and growth inhibition (D) of HepG2 cells treated with the indicated concentrations of FLV and FLV-SNEDs for 24 h and assessed using SRB cytotoxicity assay. (E) Percentage of cell death of MDA-MB-231 cells treated with vehicle, FLV, or FLV-SNEDs were determined using PI FACS analysis. (F) Western blot analysis of p53 level in MDA-MB-231 cells following their treatment with vehicle, FLV-SNED, and FLV. Vinculin was used a protein loading control. (G) Densitometric quantitation of normalized p53 level of lysates of MDA-MB-231 cells following their treatment with vehicle, FLV-SNED, and FLV. \*: Statistical significance as compared to the corresponding concentrations of FLV-treated cells assessed using two-way ANOVA followed by Bonferonni *post hoc* test. <sup>a,b</sup>: Statistical significance as compared to vehicle and FLV-treated cells respectively and assessed using one-way ANOVA followed by Tukey's *post hoc* test. S.E, Error bars; FLV, fluvastatin; SNED, self-nanoemulsifying delivery system

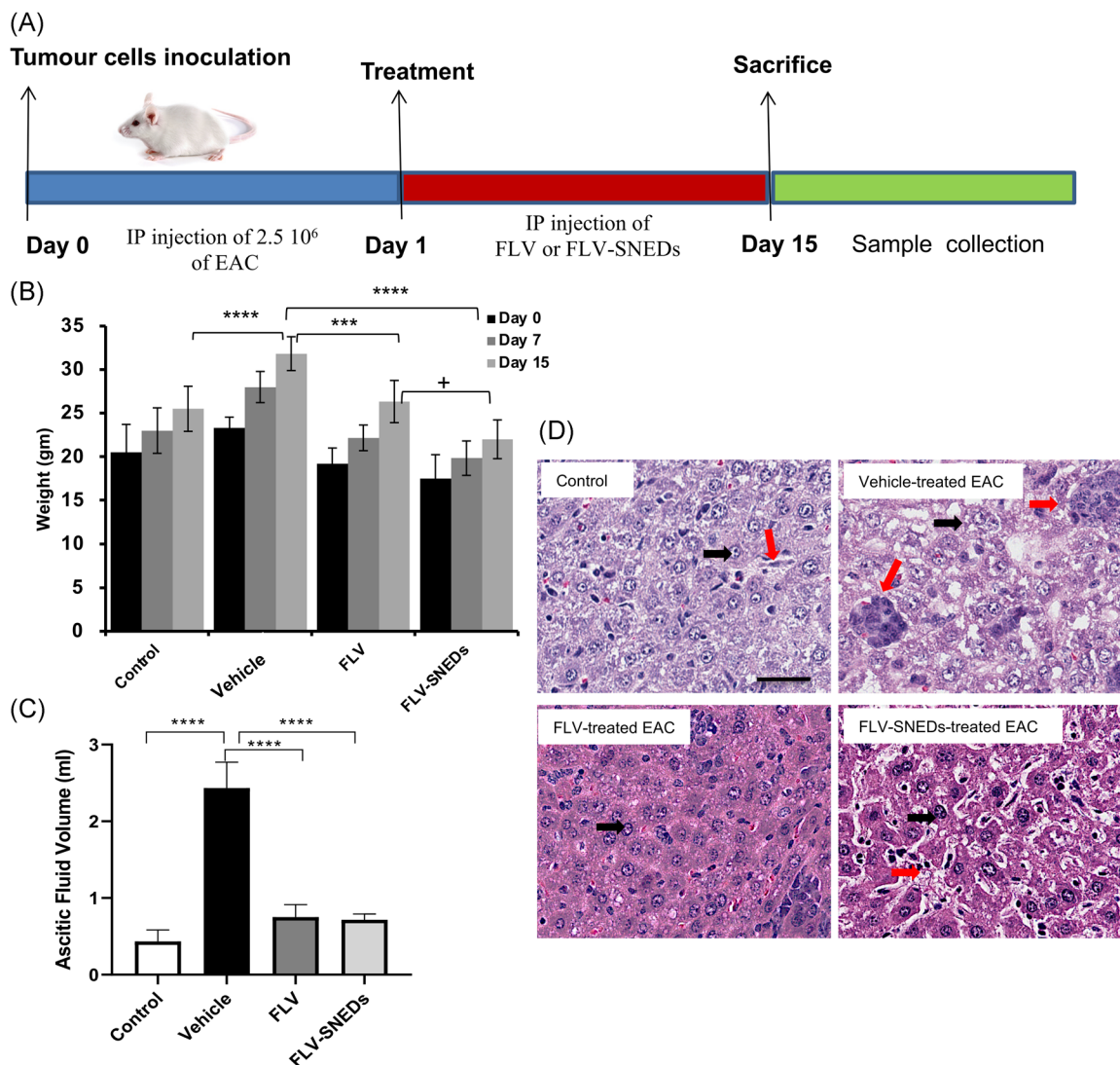


**FIGURE 3** Effect of FLV and FLV-SNEDs on the weight and ascitic fluid associated with EAC transplanted mice. (A) Schematic representation of the experimental protocols. (B) Body weight of the treated mice at different time points (0, 7, and 15 days). \*\*\*\*:  $P < 0.0001$  vehicle-treated EAC versus control (non-EAC transplanted) or FLV-SNEDs-treated EAC; \*\*\*:  $P < 0.001$  vehicle-treated EAC versus FLV-treated EAC; + $P < 0.05$  FLV-treated EAC versus FLV-SNEDs-treated EAC. (C) Volume of ascitic fluid of treated mice after 15 days. \*\*\*\*:  $P < 0.0001$  vehicle-treated EAC versus control; \*\*\*\*:  $P < 0.0001$  vehicle-treated EAC versus FLV-treated EAC and FLV-SNEDs-treated EAC. (D) Histopathological examination (H&E) of liver sections. Control group showing normal liver cords (black arrow) and liver sinusoids (red arrow). Vehicle-treated EAC group showing cohesive groups of malignant epithelial cells (red arrow) with nuclear hyperchromatism and pleomorphism (black arrow). FLV-treated EAC group showing high-grade dysplastic changes (black arrow) while the FLV-SNEDs-treated EAC group recovered the normal histological structure as normal sinusoids (red arrow) and mild large cell atypia (black arrow). Bar,  $200 \mu\text{m}$ . Ten mice per group. S.E, Error bars; EAC, Ehrlich ascites carcinoma; FLV, fluvastatin; SNED, self-nanoemulsifying delivery system

proliferating cells. Elevated Ki-67 expression is associated with increased risk of relapse and poor survival in patients with early breast cancer.<sup>49</sup> To this end, we sought to analyze the expression level of Ki-67 in EAC/liver specimens of different treatment groups. Indeed, immunohistochemical examination depicted a significantly higher percent of Ki-67 +ve tumor/EAC cells in vehicle-treated EAC as compared to the control group (Figure 4A,B). Conversely, administration of FLV or

FLV-SNEDs evidently reduced the percent of Ki-67 +ve EAC cells by 57.5% and 86.5% as compared to the vehicle-treated EAC group (Figure 4A,B).

To characterize the signaling pathways underlying the anticancer activities of FLV and FLV-SNEDs in vivo, we sought to investigate the potential involvement of apoptosis. To this end, the levels of diverse apoptotic regulators and/or mediators were measured. B-cells leukemia/lymphoma 2 (Bcl-2) is one of the crucial

apoptosis-regulatory genes which contributes to carcinogenesis by blocking programmed apoptotic cell death. Previous studies have reported that serum Bcl-2 levels might present a useful prognostic biomarker for cancer

**TABLE 1** Assessment of liver functions in different studied groups

| Parameter Groups      | ALT (I/U)               | AST (I/U)               |
|-----------------------|-------------------------|-------------------------|
| Control               | 39 ± 1.2                | 57 ± 1.5                |
| Vehicle-treated EAC   | 67 ± 1.7 <sup>a</sup>   | 86 ± 0.9 <sup>a</sup>   |
| FLV-treated EAC       | 44 ± 1.8 <sup>a,b</sup> | 39 ± 0.6 <sup>a,b</sup> |
| FLV-SNEDs-treated EAC | 41 ± 0.9 <sup>b</sup>   | 48 ± 1.2 <sup>a,b</sup> |

Note: Values are presented as mean ± S.E.

Abbreviations: EAC, Ehrlich ascites carcinoma; FLV, fluvastatin; SNED, self-nanoemulsifying delivery system.

<sup>a</sup>Change in value compared to the control group.

<sup>b</sup>Change in value compared to the vehicle-treated EAC group.

**TABLE 2** Assessment of kidney functions in different studied groups

| Parameter Groups      | Urea (mg/dl)              | Creatinine (mg/dl)        |
|-----------------------|---------------------------|---------------------------|
| Control               | 36.8 ± 1.3                | 0.7 ± 0.02                |
| Vehicle-treated EAC   | 87.3 ± 2.1 <sup>a</sup>   | 5.6 ± 0.1 <sup>a</sup>    |
| FLV-treated EAC       | 54.6 ± 2.9 <sup>a,b</sup> | 3.9 ± 0.08 <sup>a,b</sup> |
| FLV-SNEDs-treated EAC | 48.1 ± 2.3 <sup>b</sup>   | 2.8 ± 0.2 <sup>a,b</sup>  |

Note: Values are presented as mean ± S.E.

Abbreviations: EAC, Ehrlich ascites carcinoma; FLV, fluvastatin; SNED, self-nanoemulsifying delivery system.

<sup>a</sup>Change in value compared to the control group.

<sup>b</sup>Change in value compared to the vehicle-treated EAC group.

**TABLE 3** Assessment of liver oxidant/antioxidant parameters in different studied groups

| Parameter Groups      | MDA (nmol/g tissue)       | NO (U/g tissue)         | CAT (U/g tissue)          |
|-----------------------|---------------------------|-------------------------|---------------------------|
| Control               | 54.2 ± 1.6                | 27 ± 1.2                | 66.2 ± 2.5                |
| Vehicle-treated EAC   | 158.1 ± 1.9 <sup>a</sup>  | 73 ± 2.1 <sup>a</sup>   | 23.5 ± 0.8 <sup>a</sup>   |
| FLV-treated EAC       | 93.2 ± 2.3 <sup>a,b</sup> | 57 ± 0.8 <sup>a,b</sup> | 33.8 ± 0.3 <sup>a,b</sup> |
| FLV-SNEDs-treated EAC | 88.1 ± 1.7 <sup>b</sup>   | 45 ± 0.9 <sup>a,b</sup> | 58.2 ± 1.9 <sup>a,b</sup> |

Note: Values are presented as mean ± S.E.

Abbreviations: EAC, Ehrlich ascites carcinoma; FLV, fluvastatin; SNED, self-nanoemulsifying delivery system.

<sup>a</sup>Change in value compared to the control group.

<sup>b</sup>Change in value compared to the vehicle-treated EAC group.

patients including breast cancer patients.<sup>50</sup> To this end, we sought to assess the serum levels of Bcl-2 in different treatment groups. Indeed, Bcl-2 levels were significantly increased in the sera of the vehicle-treated EAC-transplanted mice by 57% as compared to the control group (Table 4). Consistent with their anticancer activities, serum Bcl-2 levels were drastically reduced by 34.5% and 47.8% in the EAC-transplanted mice which were treated with FLV or FLV-SNEDs, respectively (Table 4). In harmony with the serum levels, the expression levels of Bcl-2 mRNA were significantly elevated by 176% in the EAC infiltrating the liver specimens (Figure 5A). In contrast, treatment of EAC-transplanted mice with FLV or FLV-SNEDs decreased Bcl-2 mRNA levels by 48% and 68%, respectively, as compared to the vehicle-treated EAC cohort (Figure 5A). Consistently, administration with FLV or FLV-SNEDs significantly activated the executioner caspase, caspase-3 by 98% and 180% compared to the vehicle-treated EAC cohort (Figure 5B,C). Collectively, these findings support the contribution of apoptotic cell death in mediating the anticancer activities of FLV and FLV-SNEDs against murine EAC model in vivo.

### 3.7 | FLV and FLV-SNEDs induce p53 expression and inhibit AKT-phosphorylation and Bcl-2 expression in vivo

We next investigated the signaling pathways that may be involved in the activation of apoptosis by FLV and FLV-SNEDs. Since p53 is known to be a critical component in apoptosis pathway, we studied the role of p53 in FLV-induced apoptosis. As shown in the western blot results, both FLV and FLV-SNEDs induced total p53 expression in liver tissue lysates

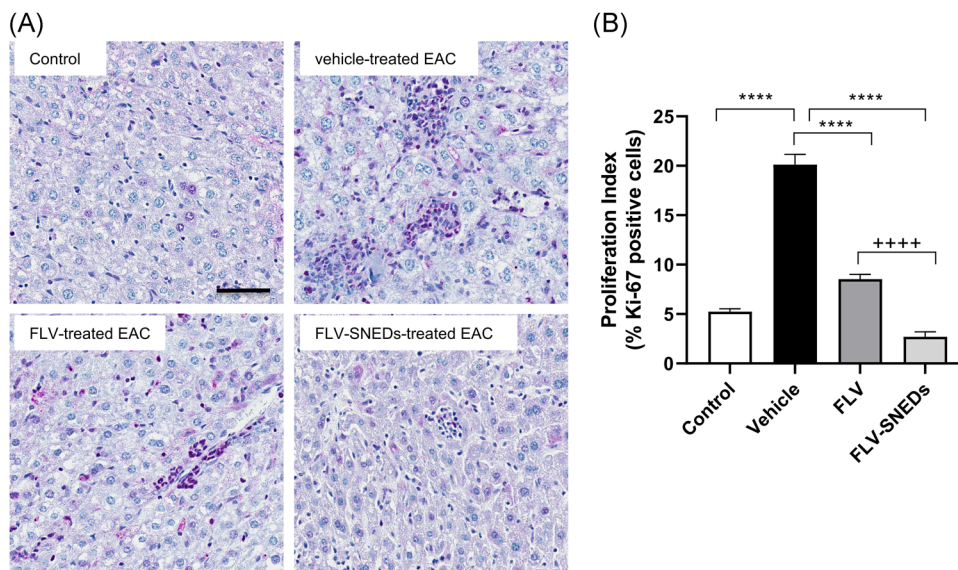


**FIGURE 4** Effect of FLV and FLV-SNEDs on tumor cell proliferation. (A) Immunohistochemical staining for Ki-67 (a marker of tumor cell proliferation) in EAC/liver specimens of different treatment groups. (B) Quantification of Ki-67. The bars show the percent of Ki-67 positive cells (12–14 fields/group). \*\*\*\*:  $P < 0.0001$  vehicle-treated EAC versus control; \*\*\*\*:  $P < 0.0001$  FLV-treated EAC versus vehicle-treated EAC; \*\*\*\*:  $P < 0.0001$  FLV-SNEDs-treated EAC versus vehicle-treated EAC and ++++:  $P < 0.0001$  FLV-SNEDs-treated EAC versus FLV-treated EAC. Bar, 100  $\mu\text{m}$ . Ten mice per group. S.E., Error bars; EAC, Ehrlich ascites carcinoma; FLV, fluvastatin; SNED, self-nanoemulsifying delivery system

**TABLE 4** Estimation of serum Bcl-2 for different studied groups

| Parameter Groups      | Bcl-2 (ng/ml)        |
|-----------------------|----------------------|
| Control               | $5.25 \pm 0.06^a$    |
| Vehicle-treated EAC   | $8.25 \pm 0.03$      |
| FLV-treated EAC       | $5.4 \pm 0.04^a$     |
| FLV-SNEDs-treated EAC | $4.3 \pm 0.09^{a,b}$ |

Note: Values are presented as mean  $\pm$  S.E.

Abbreviations: EAC, Ehrlich ascites carcinoma; FLV, fluvastatin; SNED, self-nanoemulsifying delivery system.

<sup>a</sup>Change in value compared to the vehicle-treated EAC group.

<sup>b</sup>Change in value compared to the control group.

(Figure 6). This was in accordance with the western blot results (Figure 2F) showing the increase in p53 level in FLV-SNEDs and FLV-treated MDA-MB-231 cells. Moreover, FLV and FLV-SNEDs downregulated the phosphorylation of AKT in EAC-bearing mice compared to vehicle-treated EAC cohort, which is another pathway for the induction of cell growth and proliferation. In parallel to these results, protein expressions of the antiapoptotic marker, Bcl-2, were reduced in FLV and FLV-SNEDs-treated EAC cohort, supporting the downregulation of the expression levels of Bcl-2 mRNA in the same cohort.

## 4 | DISCUSSION

The anticancer effects of FLV have been documented in a variety of cancers, although the molecular mechanisms of statin-regulated innate immune responses and cell proliferation are not well known. Therefore, we previously examined the molecular interactions of FLV and FLV-SNEDs treatment on breast cancer cells, MCF7, through autophagosome formation accompanied by lysosomal degradation.<sup>14</sup> In this study, we undertook to investigate the potential anticancer activity of both FLV and FLV-SNEDs against other aggressive subtypes of cancer with limited treatment options as TNBC and hepatocellular carcinoma (HepG2) in vitro as well as in vivo in the EAC-mice model. In our study, we demonstrate that FLV-SNEDs reduce the survival and proliferative potential of MDA-MB-231 and HepG2 cells in a concentration-dependent pattern compared to FLV (Figure 2). FLV and FLV-SNEDs impair the growth of murine mammary adenocarcinoma model in vivo (Figure 3). Moreover, p53, AKT-mTOR signaling cascades were also tested to emphasize the molecular mechanisms of FLV- and FLV-SNEDs-actions in triggering apoptotic cell death.

Numerous studies have shown that statins have a role in tumor growth inhibition and in inducing cell death in several cancer cells in a cell type-dependent manner.<sup>26,51–53</sup> These previous data are consistent with our

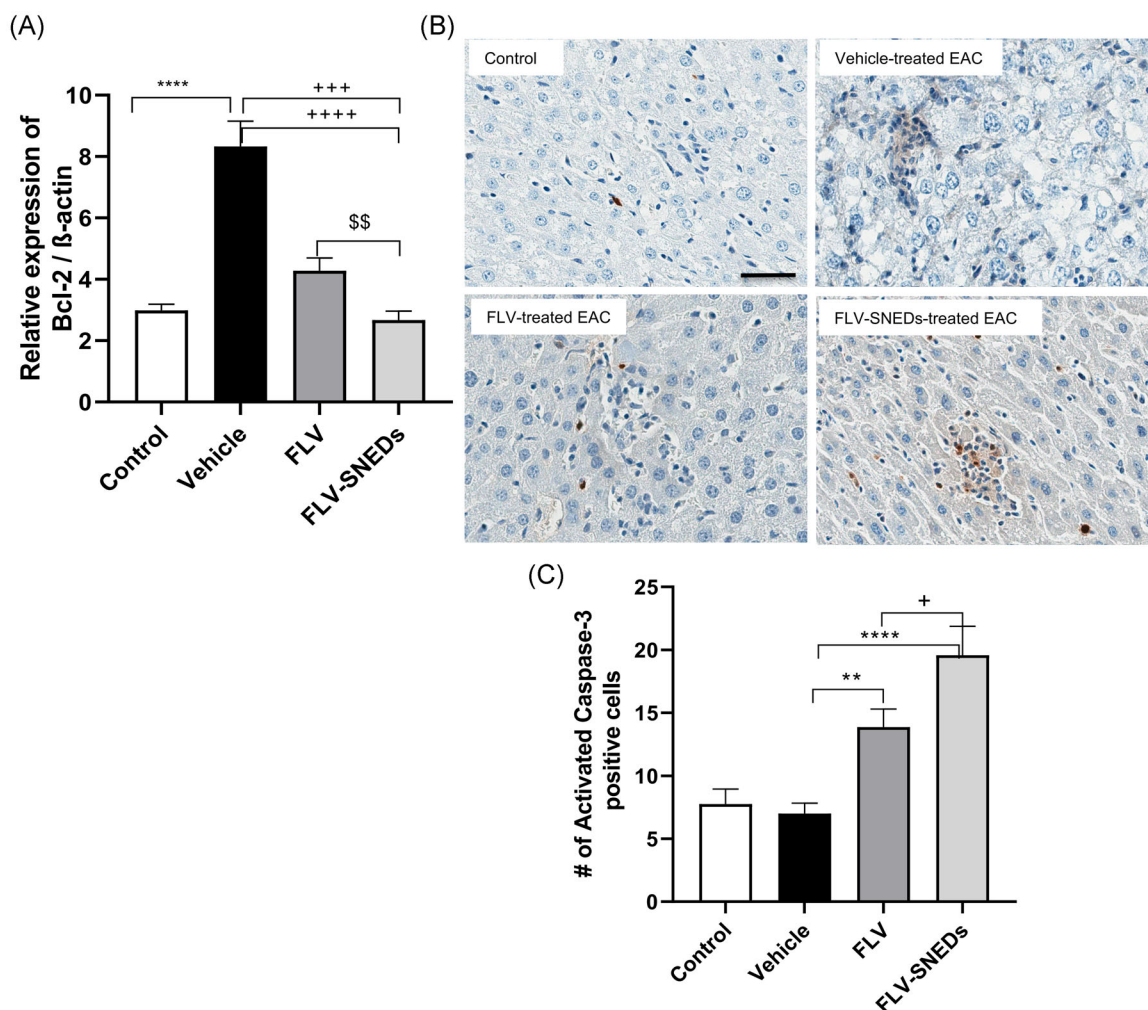


**FIGURE 5** Effect of FLV and FLV-SNEDs on apoptotic cell death. (A) Expression of Bcl-2 gene in the liver tissues exposed to FLV or FLV-SNEDs after transplantation with EAC determined by quantitative RT-PCR. \*\*\*\*:  $P < 0.0001$  vehicle-treated EAC versus control; +++:  $P < 0.001$  FLV-treated EAC versus vehicle-treated EAC; +++++:  $P < 0.0001$  FLV-SNEDs-treated EAC versus vehicle-treated EAC and \$\$:  $P < 0.01$  FLV-SNEDs-treated EAC versus FLV-treated EAC. (B) Immunohistochemical staining images of cleaved-caspase 3 protein in liver tissues. Control and vehicle-treated groups show negative expression. FLV-treated EAC shows few nuclei exhibit positive stained and FLV-SNEDs-treated EAC donates more positive expression indicated with stained nuclei with brown color. (C) Quantification of cleaved caspase-3. The bars show the number of cleaved caspase-3 positive cells (12–14 fields/group). \*\*:  $P < 0.01$  FLV-treated EAC versus vehicle-treated EAC; \*\*\*\*:  $P < 0.0001$  FLV-SNEDs-treated EAC versus vehicle-treated EAC and +:  $P < 0.05$  FLV-SNEDs-treated EAC versus FLV-treated EAC. Bar, 100  $\mu$ m. Ten mice per group. S.E., Error bars; EAC, Ehrlich ascites carcinoma; FLV, fluvastatin; SNED, self-nanoemulsifying delivery system

results showing that FLV, induced significant inhibition of the viability of MDA-MB-231 and HepG2. We next documented that apoptosis was responsible for FLV-induced cytotoxicity toward MDA-MB-231, HepG2, and EAC-bearing mice using flow cytometry, propidium iodide staining, and cleaved caspase-3 staining, indicating that FLV treatment may directly or indirectly induce apoptotic death in vivo and in vitro. Interestingly, FLV-SNEDs were more effective than FLV for regulation of cancer cell viability both in vitro as shown in MDA-MB-231 and HepG2, and in vivo in EAC-bearing mice model.

AKT, ERK, and p38 signaling pathways have been shown to be necessary for cell cycle progression and proliferation.<sup>54</sup> Previously, activation of mitogen-activated protein kinases (MAPK) cascades, including ERK1/2 was investigated in MCF-7 cells treated with FLV. FLV and FLV-SNEDs markedly suppressed the activation of ERK1/2.<sup>14</sup> PI3K/AKT/mTOR is well-known pathway in regulating apoptosis. The intrinsic pathway of apoptosis deals with mitochondrial pathway.<sup>55</sup> AKT acts as an antiapoptotic factor that directly or indirectly (via mTORC1) antagonizes cell

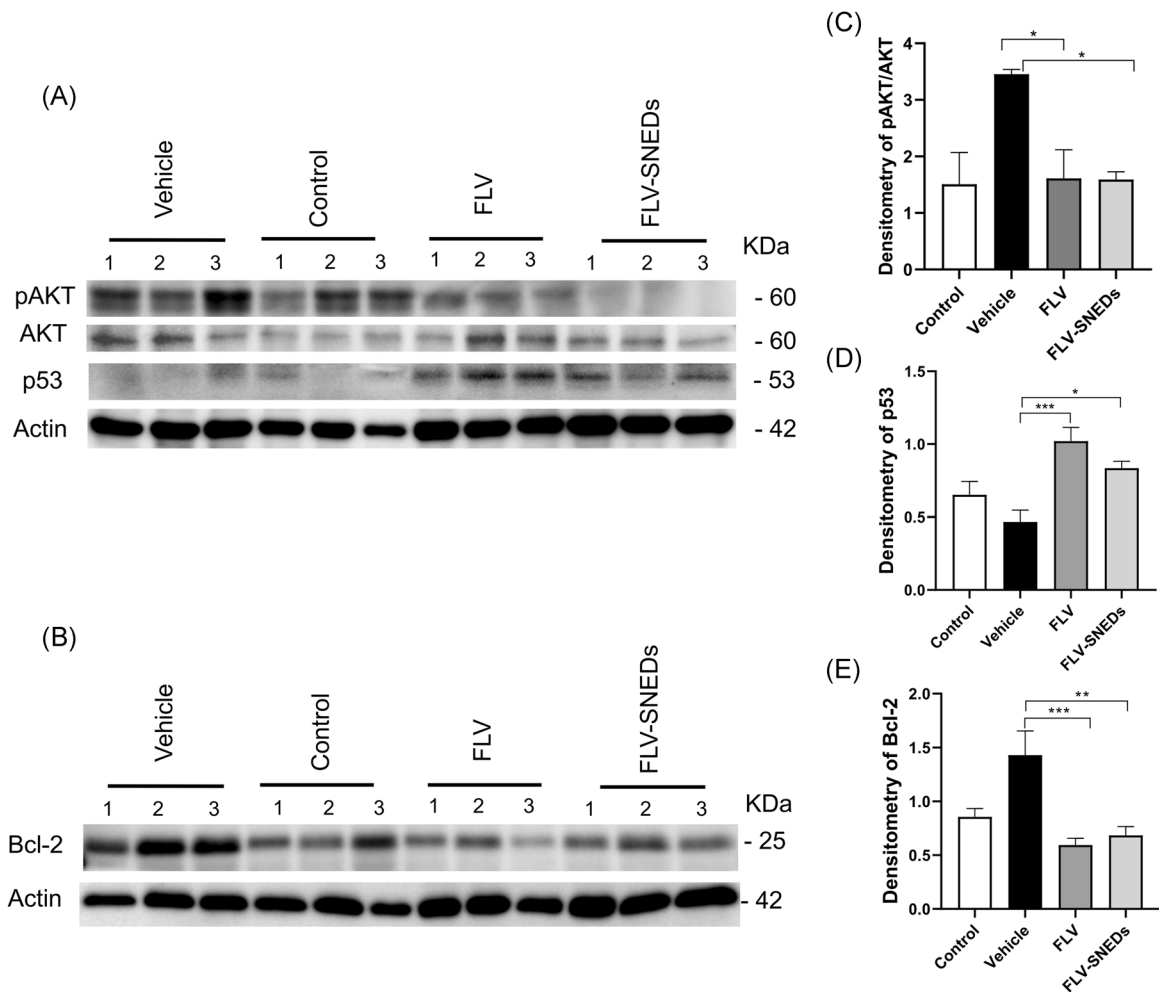


**FIGURE 6** Effect of FLV and FLV-SNEDs on p53, Akt, and Bcl-2 signaling. (A) Liver tissue lysates from all cohorts were immunoblotted with antibodies to pAkt, Akt, and p53. Representative immunoblots of corresponding proteins. Actin served as a loading control. (B) The same lysates were immunoblotted with antibodies to Bcl-2. Representative immunoblots of corresponding proteins. Actin served as a loading control. (C) Densitometric quantification of pAkt/Akt. \*:  $P < 0.05$  FLV- and FLV-SNEDs-treated EAC versus vehicle-treated EAC. (D) Densitometric quantification of p53. \*\*\*:  $P < 0.001$  FLV-treated EAC versus vehicle-treated EAC. \*:  $P < 0.05$  FLV-SNEDs-treated EAC versus vehicle-treated. (E) Densitometric quantification of Bcl-2. \*\*:  $P < 0.01$  FLV- and FLV-SNEDs-treated EAC versus vehicle-treated EAC. Three experiments were performed in duplicate. S.E., Error bars; EAC, Ehrlich ascites carcinoma; FLV, fluvastatin; SNED, self-nanoemulsifying delivery system

death signal transduction via the mitochondrial pathway.<sup>56</sup> Notably, in this study, the phosphorylation of AKT (Ser 473) was inhibited in FLV and FLV-SNEDs-treated mice (Figure 6E), indicating that inhibition of AKT phosphorylation is involved in FLV-induced apoptotic cell death. This finding is in accordance with a previous study by Qi et al.,<sup>57</sup> who showed that FLV-inhibited activation of AKT and ERK pathways were markedly blocked by mevalonate.

There is growing evidence that statins exert direct antiproliferative and proapoptotic actions on different types of human cancer cells.<sup>58</sup> Consistently, FLV and FLV-SNEDs were able to inhibit proliferation. Reduction in EAC tumor proliferation (Ki-67, proliferation marker)

is associated with an increase in tumor apoptosis (cleaved caspase-3 [CC3]) after FLV treatment. To clarify the role of p53 in FLV-induced apoptosis pathway in vitro and in vivo, we employed immunoblotting of the lysates from MDA-MB-2cells and liver tissues. We illustrate that FLV and FLV-SNEDs induce p53 expression (Figures 2 and 6). Stabilization and accumulation of p53 in the cytoplasm associated with BCL-xL leading to the release of cytochrome c from the outer-mitochondrial membrane activating pro-caspase 9 which activates caspase-3.<sup>59</sup> Thus, immunohistochemical staining of cleaved caspase-3 was increased in liver tissues from FLV- and FLV-SNEDs-treated groups (Figure 5B, C). These findings support the role of p53 in underlying the

molecular aspects of FLV and FLV-SNEDs -actions in triggering apoptotic cell death.

Finally, based on the abovementioned results, liver and kidney functions were compromised in EAC (Tables 1 and 2). This could be explained by the existence of hepatic and renal damage caused by cancer cell invasion.<sup>3</sup> Indeed, the growth and invasion of tumor cells cause interruptions in antioxidant activities by the generation of large quantities of free radicals, which may contribute to tissues damage and mutation. Accordingly, there is a positive correlation between alterations in antioxidant mechanisms and cancer cell proliferation. In this study, the liver oxidant (nitric oxide [NO] and MDA) and antioxidants (Catalase) parameters were improved in liver tissues from FLV-treated EAC-bearing mice. These findings demonstrate that FLV decreases the oxidation stress ratio (oxidant /antioxidant parameters) and thus inhibits the generation of ROS which is the precursor for tumor progression.<sup>60</sup>

## 5 | CONCLUSIONS

Daily oral intake of 20 mg/kg FLV or FLV-SNEDs produced significant *in vivo* antitumor effects in Ehrlich-bearing mice. The antitumor effect was due to FLV- or FLV-SNEDs-induced decline in tumor cell proliferation marker, Ki-67, and stimulation of apoptosis via upregulation of p53 and cleaved caspase-3 staining. FLV-SNEDs are more effective than FLV for regulation of cancer cell viability via activation of programmed cell death. These postulations confirmed the potentiality of SNEDs as a nanocarrier for anticancer drugs owing to their enhancement of anticancer efficacy and bioavailability.

## CONFLICTS OF INTEREST

The authors declare no conflicts of interest.



## ETHICS STATEMENT

The whole experimental methods were performed in accordance with the relevant guidelines of the ethical care, the experimental design and treatment of the animals underwent the regulations of the ethical committee of National Research Centre, Dokki, Cairo, Egypt.

## DATA AVAILABILITY STATEMENT

The data that support the findings of this study are available from the corresponding author upon request.

## ORCID

Hanan Elimam  <http://orcid.org/0000-0003-2585-9957>  
Khalid M. El-Say  <https://orcid.org/0000-0002-5539-3193>

## REFERENCES

1. Fitzmaurice C, Allen C, Barber C, et al. Global, regional, and national cancer incidence, mortality, years of life lost, years lived with disability, and disability-adjusted life-years for 32 cancer groups, 1990 to 2015: a systematic analysis for the global burden of disease study. *JAMA Oncol.* 2017;3(4):524-548.
2. Ozaslan M, Karagoz ID, Kilic IH, Guldur ME. Ehrlich ascites carcinoma. *Afr J Biotechnol.* 2011;10(13):2375-2378.
3. Medhat D, Hussein J, El-Naggar ME, et al. Effect of Au-dextran NPs as anti-tumor agent against EAC and solid tumor in mice by biochemical evaluations and histopathological investigations. *Biomed Pharmacother.* 2017;91:1006-1016.
4. Thurnher M, Nussbaumer O, Gruenbacher G. Novel aspects of mevalonate pathway inhibitors as antitumor agents. *Clin Cancer Res.* 2012;18(13):3524-3531.
5. Jiang P, Mukthavaram R, Chao Y, et al. *In vitro* and *in vivo* anticancer effects of mevalonate pathway modulation on human cancer cells. *Br J Cancer.* 2014;111(8):1562-1571.
6. Ahmed TA, Elimam H, Alrifai AO, et al. Rosuvastatin lyophilized tablets loaded with flexible chitosomes for improved drug bioavailability, anti-hyperlipidemic and antioxidant activity. *Int J Pharm.* 2020;588:119791.
7. Van Wyhe RD, Rahal OM, Woodward WA. Effect of statins on breast cancer recurrence and mortality: a review. *Breast Cancer.* 2017;9:559-565.
8. Safwat S, Ishak RA, Hathout RM, Mortada ND. Statins anticancer targeted delivery systems: re-purposing an old molecule. *J Pharm Pharmacol.* 2017;69(6):613-624.
9. Koyuturk M, Ersoz M, Altioek N. Simvastatin induces apoptosis in human breast cancer cells: p53 and estrogen receptor independent pathway requiring signalling through JNK. *Cancer Lett.* 2007;250(2):220-228.
10. Shen YY, Yuan Y, Du YY, Pan YY. Molecular mechanism underlying the anticancer effect of simvastatin on MDA-MB-231 human breast cancer cells. *Mol Med Rep.* 2015;12(1):623-630.
11. Yang PM, Liu YL, Lin YC, Shun CT, Wu MS, Chen CC. Inhibition of autophagy enhances anticancer effects of atorvastatin in digestive malignancies. *Cancer Res.* 2010;70(19):7699-7709.
12. Misirkic M, Janjetovic K, Vucicevic L, et al. Inhibition of AMPK-dependent autophagy enhances *in vitro* anti-glioma effect of simvastatin. *Pharmacol Res.* 2012;65(1):111-119.
13. Kang M, Jeong CW, Ku JH, Kwak C, Kim HH. Inhibition of autophagy potentiates atorvastatin-induced apoptotic cell death in human bladder cancer cells *in vitro*. *Int J Mol Sci.* 2014;15(5):8106-8121.
14. Elimam H, El-Say KM, Cybulsky AV, Khalil H. Regulation of autophagy progress via lysosomal depletion by fluvastatin nanoparticle treatment in breast cancer cells. *ACS Omega.* 2020;5(25):15476-15486.
15. Garwood ER, Kumar AS, Baehner FL, et al. Fluvastatin reduces proliferation and increases apoptosis in women with high grade breast cancer. *Breast Cancer Res Treat.* 2010;119(1):137-144.
16. Yang Z, Su Z, DeWitt JP, et al. Fluvastatin prevents lung adenocarcinoma bone metastasis by triggering autophagy. *EBioMedicine.* 2017;19:49-59.

17. Ishikawa S. Statins inhibit tumor progression via an enhancer of zeste homolog 2-mediated epigenetic alteration in colorectal cancer. *Int J Cancer*. 2014;135(11):2528-2536.
18. Aldawsari HM, Elfaky MA, Fahmy UA, Aljaeid BM, Al-Shareef OA, El-Say KM. Development of a fluvastatin-loaded self-nanoemulsifying system to maximize therapeutic efficacy in human colorectal carcinoma cells. *J Drug Delivery Sci Technol*. 2018;46:7-13.
19. Shakeel F, Raish M, Anwer MK, Al-Shdefat R. Self-nanoemulsifying drug delivery system of sinapic acid: *in vitro* and *in vivo* evaluation. *J Mol Liq*. 2016;224:351-358.
20. Shakeel F, Iqbal M, Ezzeldin E. Bioavailability enhancement and pharmacokinetic profile of an anticancer drug ibrutinib by self-nanoemulsifying drug delivery system. *J Pharm Pharmacol*. 2016;68(6):772-780.
21. Bali V, Ali M, Ali J. Nanocarrier for the enhanced bioavailability of a cardiovascular agent: *in vitro*, pharmacodynamic, pharmacokinetic and stability assessment. *Int J Pharm*. 2011;403(1-2):46-56.
22. Pouton CW. Lipid formulations for oral administration of drugs: non-emulsifying, self-emulsifying and 'self-microemulsifying' drug delivery systems. *Eur J Pharm Sci*. 2000;11(Suppl 2):S93-S98.
23. Abdel-Aziz AK, Azab SS, Youssef SS, El-Sayed AM, El-Demerdash E, Shouman S. Modulation of imatinib cytotoxicity by selenite in HCT116 colorectal cancer cells. *Basic Clin Pharmacol Toxicol*. 2015;116(1):37-46.
24. Holbeck SL, Collins JM, Doroshow JH. Analysis of Food and Drug Administration-approved anticancer agents in the NCI60 panel of human tumor cell lines. *Mol Cancer Ther*. 2010;9(5):1451-1460.
25. Abdel-Aziz AK, Pallavicini I, Ceccacci E, et al. Tuning mTORC1 activity dictates the response of acute myeloid leukemia to LSD1 inhibition. *Haematologica*. 2020;105(8):2105-2117.
26. Campbell MJ, Esserman LJ, Zhou Y, et al. Breast cancer growth prevention by statins. *Cancer Res*. 2006;66(17):8707-8714.
27. AbdElwahab AH, Yousuf AF, Ramadan BK, Elimam H. Comparative effects of *Stevia rebaudiana* and Aspartame on hepato-renal function of diabetic rats: biochemical and histological approaches. *J Appl Pharm Sci*. 2017;7(8):34-42.
28. Tesana S, Takahashi Y, Sithithaworn P, et al. Ultrastructural and immunohistochemical analysis of cholangiocarcinoma in immunized Syrian golden hamsters infected with *Opisthorchis viverrini* and administered with dimethylnitrosamine. *Parasitol Int*. 2000;49(3):239-251.
29. Zhu L, Yebra N, Retana D, et al. A drug-screening platform based on organotypic cultures identifies vulnerabilities to prevent local relapse and treat established brain metastasis. *bioRxiv*. 2020.
30. Courade JP, Angers R, Mairet-Coello G, et al. Epitope determines efficacy of therapeutic anti-Tau antibodies in a functional assay with human Alzheimer Tau. *Acta Neuropathol*. 2018;136(5):729-745.
31. Elimam H, Papillon J, Guillemette J, Navarro-Betancourt JR, Cybulsky AV. Genetic ablation of calcium-independent phospholipase A2gamma exacerbates glomerular injury in adriamycin nephrosis in mice. *Sci Rep*. 2019;9(1):16229.
32. Reitman S, Frankel S. A colorimetric method for the determination of serum glutamic oxalacetic and glutamic pyruvic transaminases. *Am J Clin Pathol*. 1957;28(1):56-63.
33. Elimam H, Ramadan B. Comparative study of the possible prophylactic and curative effects of flaxseed oil on the lipid profile and antioxidant status of hyperlipidaemic rats. *J Appl Pharm*. 2018;10(1):1000257.
34. Marsh WH, Fingerhut B, Miller H. Automated and manual direct methods for the determination of blood urea. *Clin Chem*. 1965;11:624-627.
35. Larsen K. Creatinine assay by a reaction-kinetic principle. *Clin Chim Acta*. 1972;41:209-217.
36. Ohkawa H, Ohishi N, Yagi K. Assay for lipid peroxides in animal tissues by thiobarbituric acid reaction. *Anal Biochem*. 1979;95(2):351-358.
37. Moshage H, Kok B, Huizenga JR, Jansen PL. Nitrite and nitrate determinations in plasma: a critical evaluation. *Clin Chem*. 1995;41(6 Pt 1):892-896.
38. Johansson LH, Borg LA. A spectrophotometric method for determination of catalase activity in small tissue samples. *Anal Biochem*. 1988;174(1):331-336.
39. Elimam H, Papillon J, Takano T, Cybulsky AV. Calcium-independent phospholipase A2gamma enhances activation of the ATF6 transcription factor during endoplasmic reticulum stress. *J Biol Chem*. 2015;290(5):3009-3020.
40. Livak KJ, Schmittgen TD. Analysis of relative gene expression data using real-time quantitative PCR and the 2(-Delta Delta C (T)) Method. *Methods*. 2001;25(4):402-408.
41. Elimam H, Papillon J, Takano T, Cybulsky AV. Complement-mediated activation of calcium-independent phospholipase A2gamma: role of protein kinases and phosphorylation. *J Biol Chem*. 2013;288(6):3871-3885.
42. Elimam H, Papillon J, Kaufman DR, et al. Genetic ablation of calcium-independent phospholipase A2gamma induces glomerular injury in mice. *J Biol Chem*. 2016;291(28):14468-14482.
43. Milik SN, Abdel-Aziz AK, Lasheen DS, Serya RAT, Minucci S, Abouzid KAM. Surmounting the resistance against EGFR inhibitors through the development of thieno[2,3-d]pyrimidine-based dual EGFR/HER2 inhibitors. *Eur J Med Chem*. 2018;155:316-336.
44. Kumar R, Saneja A, Panda AK. An Annexin V-FITC-propidium iodide-based method for detecting apoptosis in a non-small cell lung cancer cell line. *Methods Mol Biol*. 2021;2279:213-223.
45. Rieger AM, Nelson KL, Konowalchuk JD, Barreda DR. Modified annexin V/propidium iodide apoptosis assay for accurate assessment of cell death. *J Vis Exp*. 2011;(50).
46. Beberok A, Wrzesniok D, Rok J, Rzepka Z, Respondek M, Buszman E. Ciprofloxacin triggers the apoptosis of human triple-negative breast cancer MDA-MB-231 cells via the p53/Bax/Bcl-2 signaling pathway. *Int J Oncol*. 2018;52(5):1727-1737.
47. Abdel-Aziz AK, Saadeldin MK, D'Amico P, et al. Preclinical models of breast cancer: two-way shuttles for immune checkpoint inhibitors from and to patient bedside. *Eur J Cancer*. 2019;122:22-41.
48. Brown GC. Reversible binding and inhibition of catalase by nitric oxide. *Eur J Biochem*. 1995;232(1):188-191.



49. de Azambuja E, Cardoso F, de Castro G, et al. Ki-67 as prognostic marker in early breast cancer: a meta-analysis of published studies involving 12,155 patients. *Br J Cancer*. 2007; 96(10):1504-1513.
50. Samy N, Ragab HM, El Maksoud NA, Shaalan M. Prognostic significance of serum Her2/neu, BCL2, CA15-3 and CEA in breast cancer patients: a short follow-up. *Cancer Biomark*. 2010;6(2):63-72.
51. Clendening JW, Penn LZ. Targeting tumor cell metabolism with statins. *Oncogene*. 2012;31(48):4967-4978.
52. Pelaia G, Gallelli L, Renda T, et al. Effects of statins and farnesyl transferase inhibitors on ERK phosphorylation, apoptosis and cell viability in non-small lung cancer cells. *Cell Prolif*. 2012;45(6):557-565.
53. Tu YS, Kang XL, Zhou JG, Lv XF, Tang YB, Guan YY. Involvement of Chk1-Cdc25A-cyclin A/CDK2 pathway in simvastatin induced S-phase cell cycle arrest and apoptosis in multiple myeloma cells. *Eur J Pharmacol*. 2011;670(2-3): 356-364.
54. Nilsson EM, Brokken LJ, Harkonen PL. Fibroblast growth factor 8 increases breast cancer cell growth by promoting cell cycle progression and by protecting against cell death. *Exp Cell Res*. 2010;316(5):800-812.
55. Engelman JA. Targeting PI3K signalling in cancer: opportunities, challenges and limitations. *Nat Rev Cancer*. 2009;9(8): 550-562.
56. Shaw RJ, Cantley LC. Ras, PI(3)K and mTOR signalling controls tumour cell growth. *Nature*. 2006;441(7092):424-430.
57. Qi XF, Zheng L, Lee KJ, et al. HMG-CoA reductase inhibitors induce apoptosis of lymphoma cells by promoting ROS generation and regulating Akt, Erk and p38 signals via suppression of mevalonate pathway. *Cell Death Dis*. 2013; 4:e518.
58. Katz MS. Therapy insight: potential of statins for cancer chemoprevention and therapy. *Nat Clin Pract Oncol*. 2005; 2(2):82-89.
59. Chipuk JE, Green DR. Dissecting p53-dependent apoptosis. *Cell Death Differ*. 2006;13(6):994-1002.
60. Ratnam DV, Ankola DD, Bhardwaj V, Sahana DK, Kumar MN. Role of antioxidants in prophylaxis and therapy: a pharmaceutical perspective. *J Control Release*. 2006;113(3):189-207.

**How to cite this article:** Elimam H, Hussein J, Abdel-Latif Y, Abdel-Aziz AK, El-Say KM. Preclinical activity of fluvastatin-loaded self-nanoemulsifying delivery system against breast cancer models: emphasis on apoptosis. *J Cell Biochem*. 2022;1-17. doi:10.1002/jcb.30238